Ceramics-Silikáty 69 (3), 341-348 (2025)
www.ceramics-silikaty.cz doi: 10.13168/cs.2025.0018

BENDING STRENGTH OF PLA- ZIRCONIA BONE FRACTURE FIXATION PLATE WITH VORONOI AND REGULAR ARCHITECTURE

#MOHAMMED HASAN*, **, ALAA ALHELAL*, **, DAVER ALİ**

*Ninavah Health Directorate, Mosul, Iraq
** Karabuk University, faculty of engineering, department of biomedical engineering, Karabuk, Turkey

#E-mail: eng.moh76@yahoo.com

Submitted January 28, 2025; accepted March 28, 2025

Keywords: Orthopaedic implant, Fracture fixation, Biomedical material, PLA, Plates, Mechanical testing

Bone fractures and defects are prevalent in orthopaedics, and implant fixation of resin materials offers a promising alternative to metallic implants in biodegradability. This study investigates the design and fabrication of bone fixation plates using additive manufacturing with different structures. Plate models were designed in four groups: Octet Regular, Tesseract Regular, Voronoi S1, and Voronoi S2. Each plate group was also designed with different porosities (40, 50, 60 and 70 %). Two resins, PLA Pro and P-CROWN V3, were utilised to fabricate the plate's specimens. Mechanical testing, including a three-point bending test, was conducted to evaluate the models. Thus, the force-deflection curve, maximum stress, and fracture energy were provided for each model. The results showed that porosity is dominant in the model's mechanical behaviour. However, the architecture of models was not as effective as their porosity; it plays an essential role in their mechanical resistance. Then, the results were discussed in detail. Among the models examined in this study, the Voronoi sample (S1-40) plate exhibits higher strength than other models. This study provides valuable insights into designing and fabricating bone fixation plates with porous structures.

INTRODUCTION

Every year, approximately 1.5 million individuals suffer from bone fractures. A bone fracture is described as a clinical condition characterised by a fragmentation in the bone [1, 2]. The primary causes of fractures are trauma (e.g., vehicle accident) and pathology (e.g., bone cancer) [3]. The majority of severe fractures require surgical implant fixation because self-healing and external fixation would be complex in cases where the fractured bone segments are far from each other [2]. It is crucial to design orthopaedic devices that successfully treat trauma in the skeletal system while avoiding harm to the patient because the bone is the tissue most transplanted into the human body following blood [4, 5].

The fundamental goal of fracture fixation is establishing stable alignment and fixation of fractured bone sections, allowing for routine healing while preserving bone function [6]. Healing of a broken bone can be achieved through different approaches depending on fracture type, including screws, internal fixation plates, and intramedullary nails, as well as external fixators and pins [7]. The selection of each of these depends on the kind, location, and complexity of the fracture, as well as the patient-specific general health conditions such as the age and bone quality [8].

Tissue engineers try to develop fracture fixation plates that mimic the host bone properties [9]. Traditional materials, like stainless steel, titanium alloys, and bioresorbable polymers, have improved the safety and effectiveness of fixation systems [10]. Titanium alloys are described as strong and lightweight in design having compatibility with the human body, which makes them excellent for internal fixation devices [11]. After joining and melting the fractured bone tighter, an ideal fixation plate should quickly be removed from the patient body. Therefore, degradable implants and fixation plates have emerged in recent years [12]. Materials degrade naturally in the body, which shows many advantages to classical implants. Only a few advantages of bridgeable fixation plates have eliminated the need for removal surgery, reducing the risk of infection, reducing stress shielding, biocompatibility, adaptability to different surgical needs, reducing the risk of metal-related complications, and promoting bone healing [12, 13].

Designing bridgeable plates with porosity is of great interest since they provide various benefits. Porous features can lessen the stiffness of the implant, reducing the stress shielding and improving the natural bone remodelling [14]. Furthermore, porosity increases vascularisation and bone ingrowth, which is essential to the implant's integration and long-term effectiveness. Despite these advantages, getting the desired porosity while retaining the implant's mechanical integrity is a delicate balance that necessitates a thorough understanding of materials science, biological mechanics, and manufacturing techniques [15]. Resin materials offer

a potential solution to overcome these disadvantages associated with metals. While bioabsorbable polymers such as polylactic acid (PLA) initially lack the required mechanical strength to fix bone fractures in highly stressed areas, reinforcing these polymers could create implants with mechanical properties comparable to cortical bones. Cortical bones have an elastic modulus ranging from approximately 6 to 20 GPa, with flexural, shear, and compressive strengths estimated at 90 – 180, 43 – 89 and 130 – 210 MPa, respectively [16]. PLA Pro resin offers advantages in terms of biocompatibility and precision, its use in resorbable fracture fixation plates. On the other hand, zirconia nanoceramic resins are composed of nano-sized ceramic particles embedded in a resin matrix. These resins combine the favourable properties of ceramics and composites, offering high mechanical strength and wear resistance [17]. Zirconia nanoceramic resins offer superior mechanical properties and durability, making them ideal for permanent implants [18]. The combination of these resins offers a balance of biodegradability, mechanical strength, and aesthetic characteristics, rendering it appropriate for many orthopaedic applications.

The geometrical parameters of a fixation plate based on fracture can vary. The standard approaches calculate the mechanical strength of plates for bulk models using experimental tests, analytical, and finite element analysis. However, the prediction of mechanical behaviour for plates with porosity architecture is not a straightforward job. This difficulty intensifies for plates with random porosity structures. For example, the experimental or theoretical estimation of deformation and stress for plates with random Voronoi architectures is challenging for researchers [19]. To this end, we designed and fabricated bone fracture fixation plates with a Voronoi architecture in this study and examined their bending behaviour experimentally. The results of this study shed light on the development and design of new fixation plates with Voronoi architecture in orthopedy.

The main aim of this work is to produce and enhance bone fracture fixation plates using a combination of PLA Pro and zirconia nanoceramic resins. These plates have both regular structures (Octet and Tesseract) and irregular structures (Voronoi S1 and S2), each with different porosity levels. The study objective is to evaluate the mechanical performance of these plates under bending stress and to identify the optimum design parameters that equilibrate the mechanical strength and flexibility. This study intends to compare the mechanical characteristics of regular and Voronoi designs at varying porosity levels using experimental three-point bending tests, examine the impact of structural randomisation on stress distribution and fracture resistance, and focus on the possibility of PLA-Zirconia composite plates as biodegradable, mechanically durable alternatives for conventional metallic implants.

EXPERIMENTAL

Design and modelling of the plates

The plate models were designed using Rhinoceros-8 with the Grasshopper Plugin. Seventeen plate models were designed, one is a bulk plate, and 16 models were divided into four groups (Octet Regular, Tesseract Regular, Voronoi Samples S1, and Voronoi Samples S2) with four different porosities (40, 50, 60 and 70 %) [20]. All the models of a plate were built based on 96 cell points. Each cell in the design is a cubic structure with a side length of 5 mm, resulting in a volume of 125 mm^3 per cell. To achieve a total plate volume of 12,000 mm^3 across all the models, for this reason, 96 cells were incorporated into the plate design. This approach ensures uniformity and consistency in the structural configuration of the plates across various models. Using Rhinoceros-8 with the Grasshopper Plugin program enables us to measure the model's porosity, specific surface area, accurate control, and manipulation of the model's architecture. A three-dimensional boundary or volume box measuring 20 mm in width, 5 mm in thickness, and 120 mm in length using the Domain Box component was selected for the Voronoi plate design, then Populate 3D component points within the box were randomly distributed. Upon this, the generation and scale of the Voronoi shape using the 3D Voronoi component are conducted. Then, the Simplify Curve component is utilised to decrease the intricacy of a curve by optimising its configuration while maintaining its general form. Afterward, the shape was extracted and refined using the Multipipe component design. This step is essential to obtain smooth, tubular forms around a network of linked curves in structures with the Voronoi architecture. The last stage involves using the Custom Preview component to finalise the geometric design, preparing it for saving and subsequent 3D printing (Figure 1).

Voronoi architectures are identified by their irregular, cellular structure. This mathematical procedure partitions a space into sections according to the closeness to a given set of seed points, yielding distinct patterns that do not conform to a repetitive lattice structure. This design is especially beneficial in orthopaedic applications because it replicates the natural porosity and mechanical characteristics of cancellous bone. The irregular cell distribution in Voronoi structures improves the load distribution, minimises the stress concentration spots, and improves the osteointegration by creating channels for vascularisation and bone ingrowth.

The models were briefly noted in terms of their architecture and porosity. For instance, the O-70 describes a model with octet architecture and 70 % porosity. Table 1 presents the geometrical parameters of the plate models. Figure 2 shows the model's final 3D model and its unit cell.

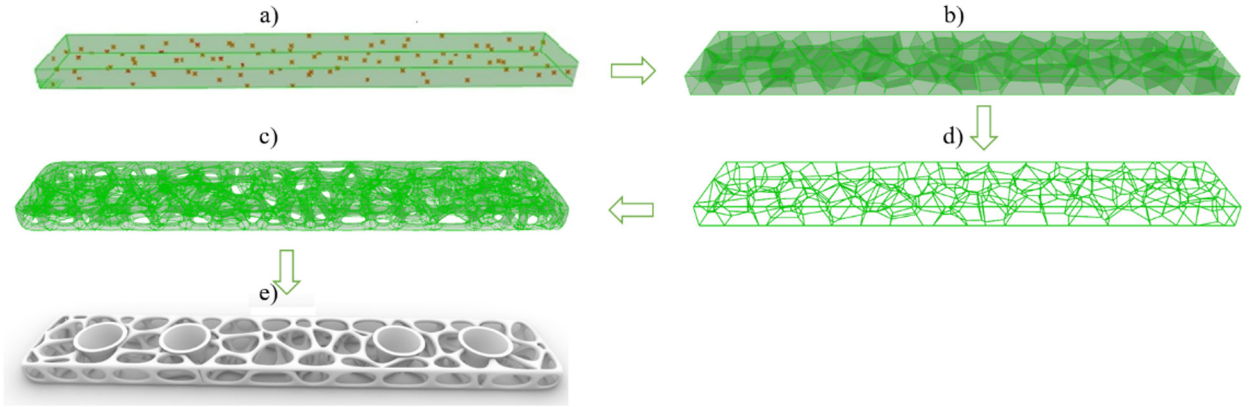

Figure 1. The steps of Voronoi plate modelling: a) Domain with the distribution of seed points, b) generation and scale Voronoi cells, c) extraction and smoothing, d) Voronoi plate three-dimensional model, and e) rendered model.

Table 1. Models' porosity and node size.

Model	Porosity (%) (T-S/T)*100	Node Size (control of porosity)
O-40	40	0.62
O-50	50	0.53
O-60	60	0.44
O-70	70	0.35
T-40	40	0.46
T-50	50	0.38
T-60	60	0.31
T-70	70	0.24
S1-40	40	0.86
S1-50	50	0.76
S1-60	60	0.63
S1-70	70	0.5
S2-40	40	0.28
S2-50	50	0.38
S2-60	60	0.49
S2-70	70	0.5

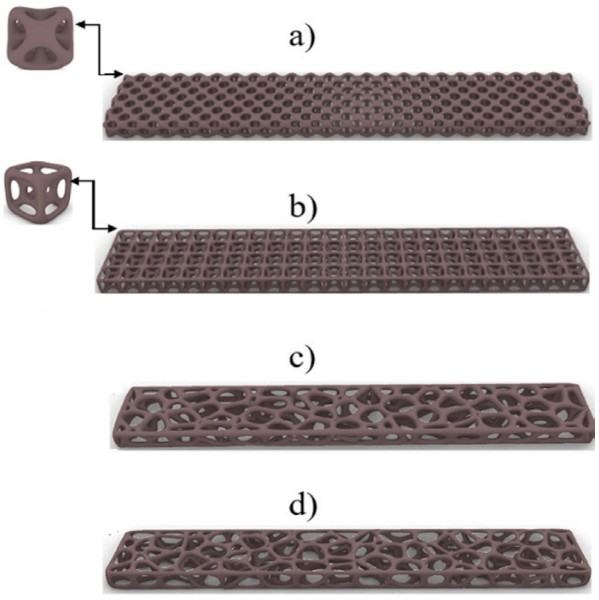

Figure 2. Plate models: a) Octet regular, b) Tesseract regular, and random structure of c) Voronoi S1 and d) Voronoi S2.

As shown in Figure 2, the Octet and Tesseract were built up from repeating a unit cell, but the plates with Voronoi architecture did not possess repeated unit cells.

Figure 3 shows all 17 plate 3D models. As can be seen, the decreasing strut thickness in each group of models left us with models with the same architecture and different porosity.

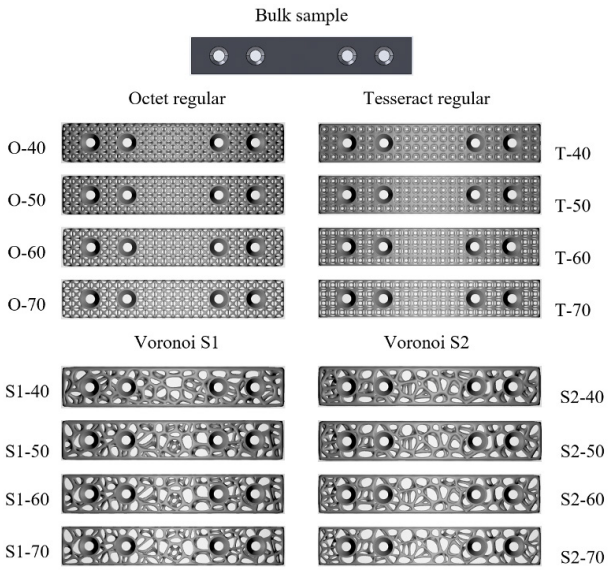

Figure 3. All the plate models: one is a bulk one, and the others are classified into four group-designed structures with four porosities designed by the Rhino program.

Manufacturing of samples

Material selection

To produce the samples using three printing techniques in this study, we used the composition of two resins: PLA Pro and zirconia nanoceramic. These resins are mixed at a mass ratio of 1:1. PLA Pro resin (eSUN eResin-PLA Pro) is a 3D printing photopolymer resin characterised by its viscosity (200 – 300 mPa s), density

(1.09 – 1.10 g·cm^{-3}), tensile strength (37 – 48 MPa), elongation at break (25 – 28 %) and hardness (Shore D 78 – 80) [21]. Zirconia nanoceramic resin (P-CROWN V3), is a biocompatible hybrid resin having high flexural strength (> 440 MPa), flexural modulus (> 9500 MPa), and minimal water absorption (< 1.2 µg·mm^{-3}) [22].

3D printing

The 3D models were saved in the STL format and prepared as input files using the Chitubox3D program for 3D printing by slicing into layers and supporting the models; this will change the file type from STL to Chitubox. Then, a Phrozen Sonic Mini 8K S resin 3D printer was used to print all the models (Figure 4) shown as printed samples. The resin is produced in high resolution using the 3D printer for precise applications. The printing parameters are presented in Table 2 [23].

Table 2. Printer and printing parameters.

Parameter	Specification
Printer Type	LCD Resin 3D Printer
Technology	UV LCD (8K Monochrome Panel)
XY Resolution	22 µm (7680 x 4320 pixels, 8K)
Layer Thickness	50 µm
Printing Speed	80 mm/h
UV light wavelength	405 nm

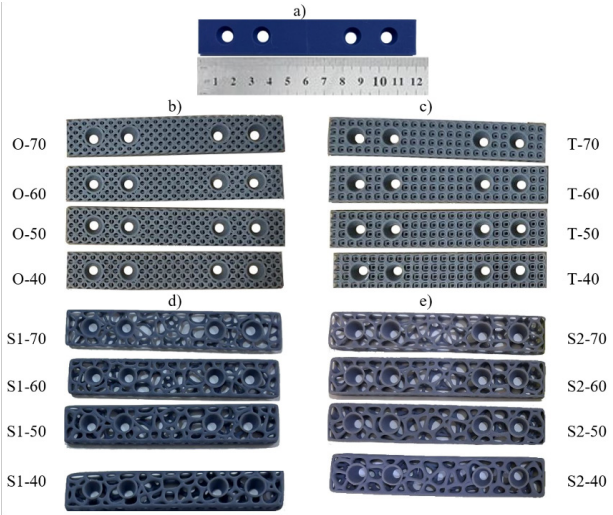

Figure 4. All the printed plate sample models: a) Bulk sample, b) Octet regular, c) Tesseract regular, d) Voronoi S1 and e) Voronoi S2 samples.

Ultrasonic cleaning

All the supports from the printed models were removed to get the final form of the samples. Then, a 99-purity alcohol solution was used to wash the samples and put them in an ultrasonic cleaner machine to remove the stuck impurities so the product was cleaned [24].

Sample curing

This post-processing can maximise the material properties, improving the parts' strength and performance. Here, we consistently used a precise combination of heat and 405 nm light to the post-cure printing [25].

Bending test

The bending strength of bone plates is important to ensure enough stability during fractured bone healing [26]. The three-point bending test is a reliable method to determine the strength of such plates [27]. Here, a three-point test to examine the bending strength of the sample was performed using a GESTER (electronic tensile testing Machine model GT-C02-1). This test allowed one to determine the maximum load the samples can tolerate before failure. All the samples were bent to the fracture point (Figure 5), and then the maximum force and deflection were determined. The machine head speed was set at 100 mm·min^{-1}.

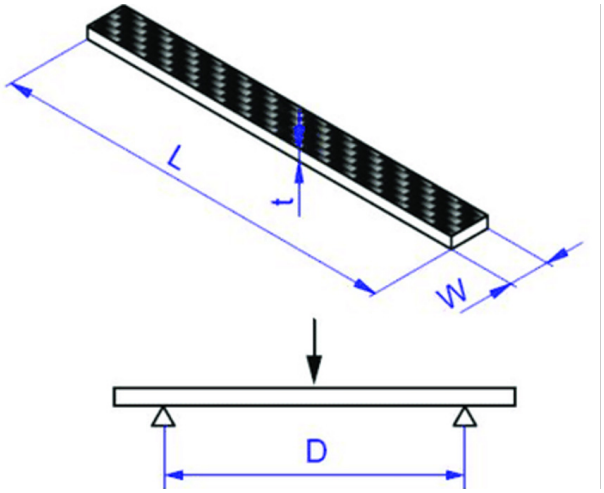

a) specimen dimensions (L = 120, D = 50, W = 20 and t = 5 mm)

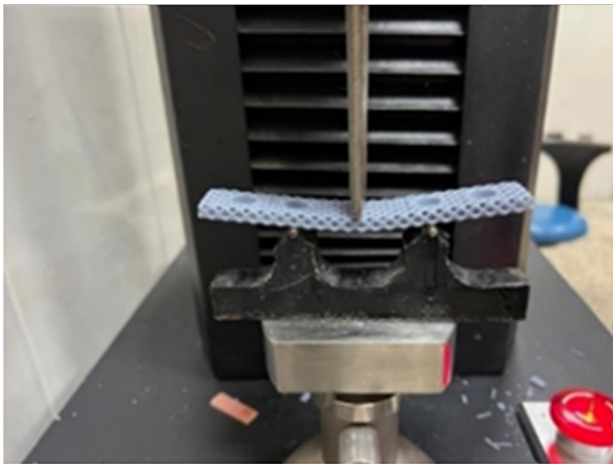

b) experimental set-up accorfing to ASTM D7264

Figure 5. 3-point bending test.

As shown in Figure 5, the sample was bent between the screw holes to avoid their effect on the models' solidity.

RESULTS AND DISCUSSION

Geometrical accuracy of the fabricated plates

Where complicated methods like micro-CT visualization are expensive techniques to evaluate the 3D printing quality of scaffolds [28], mass measuring is a straightforward approach to understanding the 3D printed samples accuracy [29]. In this study, to probe the printing accuracy of the 3D models and printed samples, their mass was measured with a 0.01 g resolution balance. The result is illustrated in Table 3. Three specimens were printed from each model, and their average mass was calculated. The CAD models' mass was calculated by multiplying their volume (which can be observed in Rhinoceros software) by the selected material density (the density of a bulk sample with the size of 10 mm^3 was calculated as 1.17 $g{\cdot}mm^{-3}$).

Table 3. The mass discrepancy between the CAD models and the printed samples.

Sample	CAD model mass (g)	Printed model mass (g)	Error (%)
S	14.04	14.84	5.69
O-40	8.34	8.78	5.3
O-50	6.94	7.17	3.3
O-60	5.61	5.95	6
O-70	4.31	4.42	2.6
T-40	8.44	9.01	6.7
T-50	6.89	7.19	4.3
T-60	5.64	5.92	5.7
T-70	4.17	4.42	6.1
S1-40	8.34	8.77	5.2
S1-50	6.98	7.36	5.4
S1-60	5.57	5.88	5.5
S1-70	4.22	4.35	3.0
S2-40	8.37	8.61	2.9
S2-50	6.90	6.99	1.3
S2-60	5.62	5.74	2.2
S2-70	4.33	4.6	6.2

As demonstrated in Table 3, the mass discrepancy between the theoretical and samples was under 7 % for all the models. Such differences between the designed model and the printed model also were reported in similar works [30, 31]. Therefore, the 3D models and fabricated samples are in agreement and ready for mechanical performance tests.

Bending test results

All 17 specimens were tested, and the force--displacement for each model was demonstrated in Figure 6. Applying force on the samples continued until a complete fracture occurred (Figure 6).

As can be seen, the bulk plate showed the highest fracture strength. In porous plates, the increase in porosity causes a lower fracture strength. We can conclude this from the decreasing trend in the force required to break the sample. For example, S1-70 yields under a force of 49 N, and from the same group of plates, model S1-40 fractured under a force of 190 N, which is approximately fourfold of the former one. A similar trend of force dependency on porosity is observable in other models, too. The amount of force required to break the sample was also affected by its architecture. For instance, S1-40 was fractured under a force of 190 N, about 50 – 60 % higher than the models with the same porosity in the rest of the groups. Moreover, the deflection of samples was affected by their porosity. The deflection of the bulk model before a complete fracture was relatively higher than that of porose plates except for S2-70, which possessed a similar deflection to the bulk model. However, like the force-porosity relation, we did not find a specific pattern between the deflection and porosity, though only in the Voronoi S2 group did the deflection increase with the increasing porosity.

Although Figure 6 shows valuable information about the model's deflection behaviour, a 3-point test calculation of maximum stress (σ_{max}) and fracture energy[32], are also important criteria to evaluate the mechanical behaviour of samples. A sample under three-point bending can be calculated by the following equation [33]:

$$\sigma_{max} = \frac{3F_{max}L}{2Wt^2} \quad (1)$$

where σ_{max}, L, W and t represent the specimen's maximum stress, maximum applied load, and geometrical parameters, respectively. The bar graphic of σ_{max} is illustrated in Figure 7.

The σ_{max} result showed the dominant porosity role in the plate's flexural strength. An increasing porosity decreased the σ_{max} in all four groups. For example, S1-40 demonstrated a 28.45 MPa of σ_{max}, approximately 4 times higher than the S1-70 model in the same group. Although the impact of architecture is not as prominent as porosity, it still plays a significant role in the mechanical behaviour of implants. For instance, S1-40 yields 28.45 MPa of σ_{max}, nearly 65 % higher than its counterparts with different architectures.

The measuring area drove the fracture energy for each model under each curve in Figure 6. The results are shown in Figure 8.

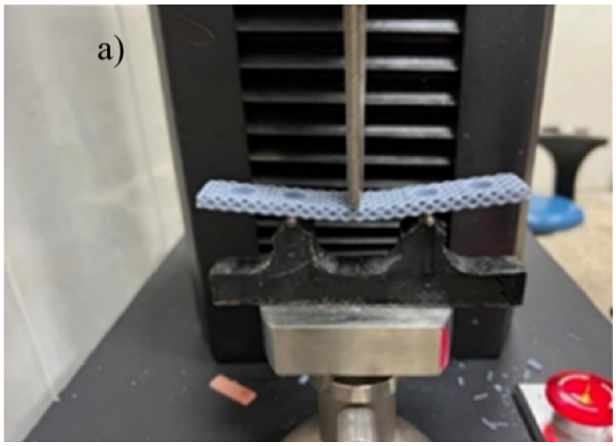

a) fracture observation

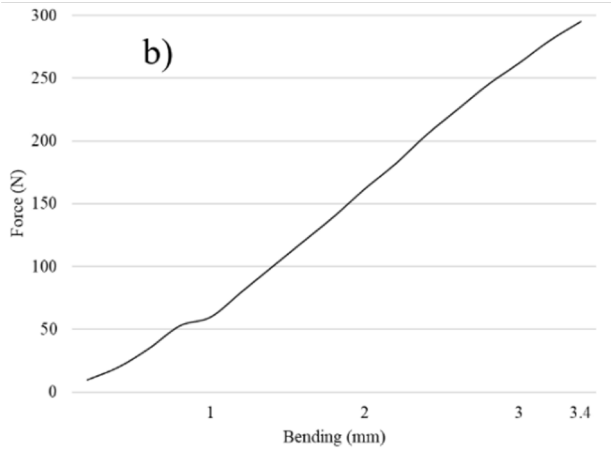

b) bulk plate

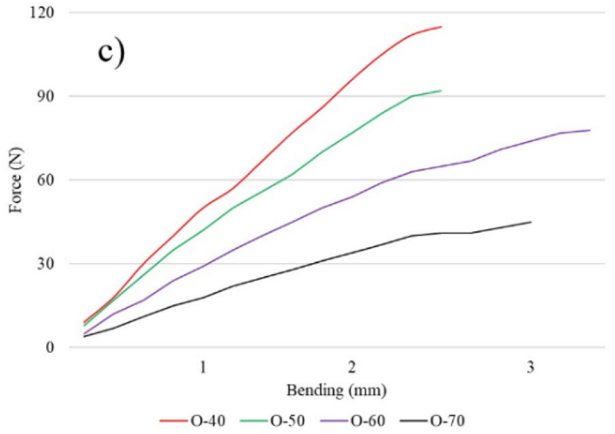

c) Octet regular

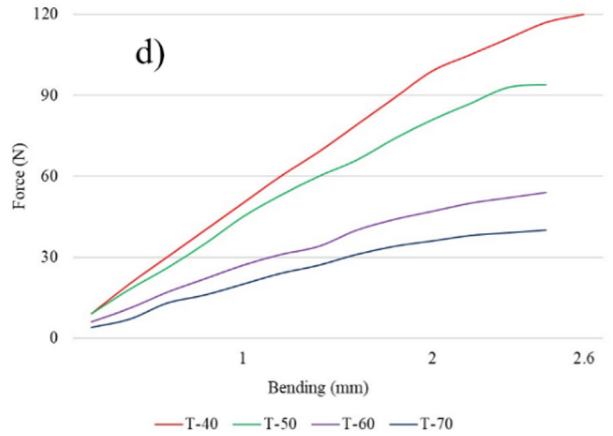

d) Tesseract regular

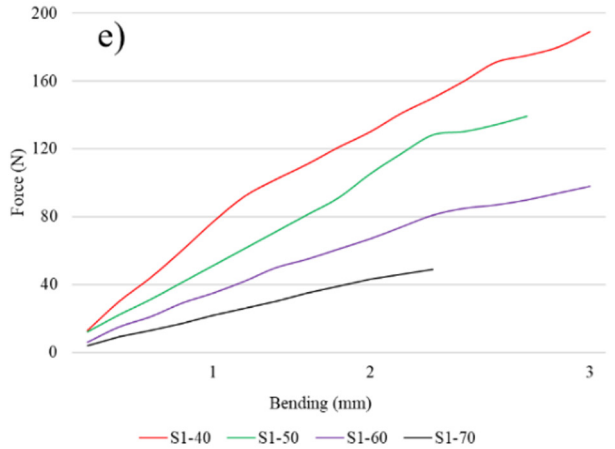

e) random structure Voronoi S1

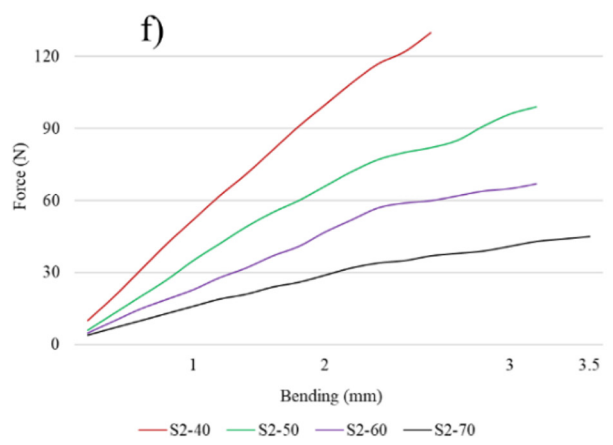

f) Voronoi S2

Figure 6. Force displacement: a) fracture observation, b) bulk plate, c) Octet regular, d) Tesseract regular, e) random structure Voronoi S1 and f) Voronoi S2 models.

The discrepancy in the fracture energy and σ_{max} between the plate models was also echoed in literature studies on the relationship between the porosity and mechanical properties. The unit cell components in periodic lattices can stretch or compress under static and dynamic loads, whereas irregular structures primarily deform through bending. Berger et al. demonstrated that plate-based lattice structures can approach the upper limits defined by the Hashin–Shtrikman bounds, representing the theoretical maximum modulus and strength of composite materials [34]. Furthermore, Crook et al. recently developed cubic-octet plate lattices that achieve these upper bounds. Plate-based lattices also show enhanced the performance in the specific energy

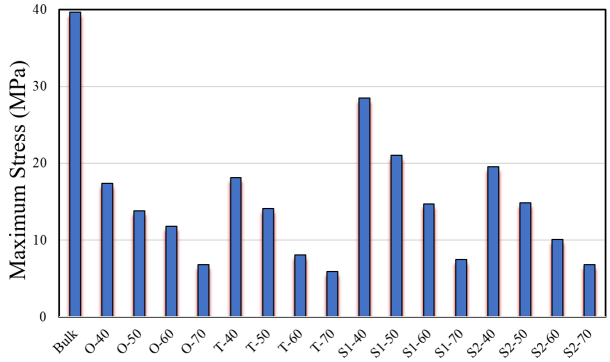

Figure 7. Maximum stress (σ_{max}) of all the models before fracture.

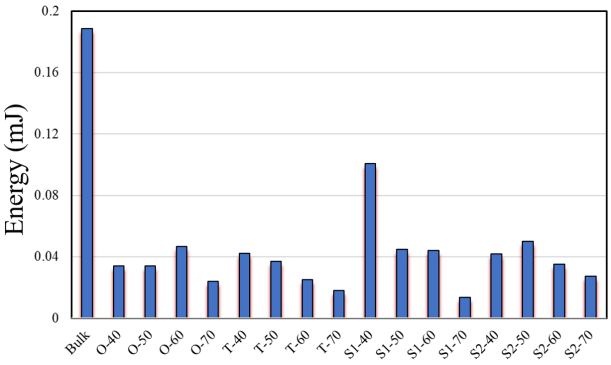

Figure 7. The fracture energy of all the models.

absorption [35]. Regarding design influence, literature studies support the findings that different designs handle porosity differently. Voronoi designs, for example, provide better structural integrity at similar porosities, while Tesseract designs offer a balance between weight reduction and mechanical strength.

The present work investigates two Voronoi model designs, S1 and S2, with porosities of 40, 50, 60 and 70 %. These models are intended to analyse the impact of randomness in structural architecture on mechanical strength under bending stress. The S1-40 model, characterised by 40 % porosity, demonstrated superior bending strength and maximum stress resistance, highlighting the structural advantages of Voronoi designs at reduced porosities.

CONCLUSIONS

The focus of the current work is on the development of a composite implant plate for bone fractures. An analysis was performed using two resin types (Polylactic Acid (PLA) Pro and P-CROWN V3 (zirconia and ceramic hybrid)) with the primary aim of optimising the plate design. Topological optimisations were performed using various mass reduction criteria while considering the structural compatibility. The outcomes of the study can be summarised below:

- PLA- Zirconia is a suitable composite for 3D printing parts with an irregular structure.
- Porosity is the dominant factor that governs the mechanical properties of the plates.
- The mechanical properties of the plates were affected by their architecture.
- In this work, the Voronoi S1 plate with 40 % porosity (S1-40) was more substantial than all the other samples tested in this study.
- Though the results of this study showed a reasonable relationship between the maximum stress and plate design, more experimental and theoretical is necessary to optimise and formulate the geometrical parameters and their effect on the mechanical properties of such implants.

REFERENCES

1. Gupta H.S., Zioupos P. (2008): Fracture of bone tissue: the 'hows' and the 'whys'. *Medical Engineering & Physics, 30*(10), 1209-1226. doi: 10.1016/j.medengphy.2008.09.007
2. Ahirwar H., Zhou Y., Mahapatra C., Ramakrishna S., Kumar P., Nanda H. S. (2020): Materials for orthopedic bioimplants: modulating degradation and surface modification using integrated nanomaterials. *Coatings, 10*(3), 264. doi: 10.3390/coatings10030264
3. Kim T., See C. W., Li X., Zhu D. (2020): Orthopedic implants and devices for bone fractures and defects: Past, present and perspective. *Engineered Regeneration, 1*, 6-18. doi: 10.1016/j.engreg.2020.05.003
4. Mugnai R., Tarallo L., Capra F., Catani F. (2018): Biomechanical comparison between stainless steel, titanium and carbon-fiber reinforced polyetheretherketone volar locking plates for distal radius fractures. *Orthopaedics & Traumatology: Surgery & Research, 104*(6), 877-882. doi: 10.1016/j.otsr.2018.05.002
5. Faour O., Dimitriou R., Cousins C. A., Giannoudis P. V. (2011): The use of bone graft substitutes in large cancellous voids: any specific needs?. *Injury, 42*, S87-S90. doi: 10.1016/j.injury.2011.06.020
6. Tian L., Tang N., Ngai T., Wu C., Ruan Y., Huang L., Qin L. (2019): Hybrid fracture fixation systems developed for orthopaedic applications: A general review. *Journal of Orthopaedic Translation, 16*, 1-13. doi: 10.1016/j.jot.2018.06.006
7. Chandra G., Pandey A., Pandey S. (2020): Design of a biodegradable plate for femoral shaft fracture fixation. *Medical Engineering & Physics, 81*, 86-96. doi: 10.1016/j.medengphy.2020.05.010
8. Compston J.E., McClung M.R., Leslie W.D. (2019): Osteoporosis seminar 2019. *The Lancet, 393*, 10169, 364-376.
9. Hady A.A.Z., Azmi L., Abdullah A.R. (2020): The Annals of Biomedical Engineering on Critical Size Bone Defect: A Review. *Malaysian Journal of Science Health & Technology, 6*. doi: 10.33102/mjosht.v6io.118
10. Al-Shalawi F.D., Mohamed Ariff A.H., Jung D.W., Mohd Ariffin M.K.A., et al. (2023): Biomaterials as implants in the orthopedic field for regenerative medicine: metal versus synthetic polymers. *Polymers, 15*(12), 2601. doi: 10.3390/

polym15122601
11. Niinomi M. (2008): Mechanical biocompatibilities of titanium alloys for biomedical applications. *Journal of the Mechanical Behavior of Biomedical Materials, 1*(1), 30-42. doi: 10.1016/j.jmbbm.2007.07.001
12. Paiva J.C., Oliveira L., Vaz M.F., Costa-de-Oliveira S. (2022): Biodegradable bone implants as a new hope to reduce device-associated infections - a systematic review. *Bioengineering, 9*(8), 409. doi: 10.3390/bioengineering9080409
13. Chandra G., Pandey A. (2020): Biodegradable bone implants in orthopedic applications: a review. *Biocybernetics and Biomedical Engineering, 40*(2), 596-610. doi: 10.1016/j.bbe.2020.02.003
14. Bandyopadhyay A., Mitra I., Avila J. D., Upadhyayula M., Bose S. (2023): Porous metal implants: processing, properties, and challenges. *International Journal of Extreme Manufacturing, 5*(3), 032014. doi: 10.1088/2631-7990/acdd35
15. Bandyopadhyay A., Mitra I., Goodman S.B., Kumar M., Bose S. (2023): Improving biocompatibility for next generation of metallic implants. *Progress in Materials Science, 133*, 101053. doi: 10.1016/j.pmatsci.2022.101053
16. DeStefano V., Khan S., Tabada A. "Applications of PLA in modern medicine," *Engineered Regeneration*, vol. 1, no. April, pp. 76–87, 2020, doi: 10.1016/j.engreg.2020.08.002.
17. Pasha M., Muhammad N., Shahnawaz S., Najmi Y., Shahroz N., Liaqat S. (2022): Ceramic nanomaterials in dental applications. *Nanoengineering of Biomaterials, 2,* 123-144. doi: 10.1002/9783527832095.ch22
18. Ceren N., Turp V., Emir F., Akgüngör G., Ayyıldız S., Şen D. (2016): Nanoceramics and hybrid materials used in CAD/CAM systems. *Aydın Dental Journal, 2*(3), 55-61.
19. Li P., Lyu F., Zhou H., Li H., et al. (2025): Controllable design and evaluation of Voronoi-based irregular porous scaffolds for bone restoration. *Materials Today Communications, 42,* 111224. doi: 10.1016/j.mtcomm.2024.111224
20. Dabrowski B., Swieszkowski W., Godlinski D., Kurzydlowski K.J. (2010): Highly porous titanium scaffolds for orthopaedic applications. *Journal of Biomedical Materials Research Part B: Applied Biomaterials, 95*(1), 53-61. doi: 10.1002/jbm.b.31682
21. Jahadakbar A., Nematollahi M., Safaei K., Bayati P., et al. (2020). Polishing of Sti ff ness-modulated porous nitinol bone fixation plates followed by thermomechanical and composition analysis. *Metals (Basel), 10*, 1-15.
22. Kongkiatkamon S., Booranasophone K., Tongtaksin A., Kiatthanakorn V., Rokaya D. (2021): Comparison of fracture load of the four translucent zirconia crowns. *Molecules, 26*(17), 5308. doi: 10.3390/molecules26175308
23. Vedhanayagam A., Golfetto M., Ram J.L., Basu A.S. (2023): Rapid micromolding of sub-100 µm microfluidic channels using an 8K stereolithographic resin 3D printer. *Micromachines, 14*(8), 1519. doi: 10.3390/mi14081519
24. Xu H., Tu J., Niu F., Yang P. (2016): Cavitation dose in an ultrasonic cleaner and its dependence on experimental parameters. *Applied Acoustics, 101*, 179-184. doi: 10.1016/j.apacoust.2015.08.020
25. Bennett J. (2017): Measuring UV curing parameters of commercial photopolymers used in additive manufacturing. *Additive Manufacturing, 18*, 203-212. doi:10.1016/j.addma.2017.10.009
26. Subasi O., Oral A., Noyan S., Tuncozgur O., Lazoglu I. (2021): In silico analysis of modular bone plates. *Journal of the Mechanical Behavior of Biomedical Materials, 124,* 104847. doi:10.1016/j.jmbbm.2021.104847
27. Liesmäki O., Plyusnin A., Kulkova J., Lassila L.V., Vallittu P.K., Moritz N. (2019): Biostable glass fibre-reinforced dimethacrylate-based composites as potential candidates for fracture fixation plates in toy-breed dogs: Mechanical testing and finite element analysis. *Journal of the Mechanical Behavior of Biomedical Materials, 96*, 172-185. doi: 10.1016/j.jmbbm.2019.04.016
28. Suchý T., Šupová M., Bartoš M., Sedláček R., Piola M., et al. (2018): Dry versus hydrated collagen scaffolds: are dry states representative of hydrated states?. *Journal of Materials Science: Materials in Medicine, 29,* 1-14. doi: 10.1007/S10856-017-6024-2
29. Hanon M.M., Zsidai L., Ma Q. (2021): Accuracy investigation of 3D printed PLA with various process parameters and different colors. *Materials Today: Proceedings, 42*, 3089-3096. doi: 10.1016/j.matpr.2020.12.1246
30. Liu H., Ahlinder A., Yassin M.A., Finne-Wistrand A., Gasser T.C. (2020): Computational and experimental characterization of 3D-printed PCL structures toward the design of soft biological tissue scaffolds. *Materials & design, 188*, 108488. doi: 10.1016/j.matdes.2020.108488
31. Wang M.O., Vorwald C.E., Dreher M.L., Mott E.J., et al. (2014): Evaluating 3D printed biomaterials as scaffolds for vascularized bone tissue engineering. *Advanced materials (Deerfield Beach, Fla.), 27*(1), 138. doi: 10.1002/adma.201403943
32. Bertocci G., Thompson A., Pierce M.C. (2017): Femur fracture biomechanics and morphology associated with torsional and bending loading conditions in an in vitro immature porcine model. J*ournal of Forensic and Legal Medicine, 52*, 5-11. doi: 10.1016/j.jflm.2017.07.021
33. Yao B., Zhou Z., Duan L., Chen Z. (2018): Characterization of three-point bending properties of metal–resin interpenetrating phase composites. *RSC Advances, 8*(29), 16171-16177. Available: https://pubs.rsc.org/en/content/articlehtml/2018/ra/c8ra01953c
34. Berger J.B., Wadley H.N.G., McMeeking R.M. (2017): Mechanical metamaterials at the theoretical limit of isotropic elastic stiffness. *Nature, 543*(7646), 533-537. doi: 10.1038/nature21075
35. Crook C., Bauer J., Guell Izard A., Santos de Oliveira C., et al. (2020). Plate-nanolattices at the theoretical limit of stiffness and strength. *Nature Communications, 11*(1), 1579. doi: 10.1038/s41467-020-15434-2